Microfluid Nanofluid (2008) 5:23–31
DOI 10.1007/s10404-007-0210-3

RESEARCH PAPER

Improvement of microchannel geometry subject to electrokinesis and dielectrophoresis using numerical simulations

Jae-Sung Kwon · Joo-Sung Maeng · Myung-Suk Chun · Simon Song

Received: 2 April 2007 / Accepted: 25 July 2007 / Published online: 24 August 2007

Abstract This paper addresses the effects of microchannel geometry with electrically insulating posts on a particle flow driven by electrokinesis and dielectrophoresis. An in-house numerical program is developed using a numerical model proposed in literature to predict particle flows in a microchannel with a circular post array. The numerical program is validated by comparing the results of the present study to those in the literature. Results obtained from a Monte-Carlo simulation confirm the three particle flow types driven by an external DC electric field: electrokinetic flow, streaming dielectrophoretic flow, and trapping dielectrophoretic flow. In addition, we study the effects of electrokinetic and dielectrophoretic forces on particle transports by introducing a ratio of lateral to longitudinal forces exerted on a particle. As a result, we propose an improved microchannel geometry to enhance particle transports across electrokinetic streamlines for a given power dissipation. The improved microchannel has a shorter longitudinal spacing between the circular posts than a reference microchannel. We also discuss the critical values of dimensionless variables that distinguish the three particle flow types for both improved and reference microchannels.

Keywords Electrokinesis · Dielectrophoresis · DC electric field · Insulating post

J.-S. Kwon
Mechanical Engineering and Technology Research Institute, Hanyang University, 17 Haengdang-dong, Seongdong-gu, Seoul 133-791, South Korea

J.-S. Maeng · S. Song (✉)
School of Mechanical Engineering, Hanyang University, 17 Haengdang-dong, Seongdong-gu, Seoul 133-791, South Korea
e-mail: simonsong@hanyang.ac.kr

M.-S. Chun
Complex Fluids Research Lab, Korea Institute of Science and Technology (KIST), PO Box 131, Cheongryang, Seoul 130-650, South Korea

1 Introduction

One of the main purposes of microfluidic chip development is the automation of analytical procedures for biochemistry. Due to intensive efforts on the development over the past decade, many analytical methods, like non-intrusive sampling, separation, and sorting have been integrated onto a microfluidic chip (Auroux et al. 2002; Reyes et al. 2002; Vilkner et al. 2004). However, sample pretreatment to process a complex solution to the desired form of target molecules is often conducted off-chip. This is because sample pretreatment techniques widely vary from one sample to another.

Electrokinesis (EK) and dielectrophoresis (DEP) have been given attention for the development of on-chip sample pretreatment techniques because they are effective in the transport and control of bio samples like DNA, RNA, protein, cell dissolution, bacterium, and virus. EK, including electroosmosis and electrophoresis, has been steadily studied since Reuss demonstrated that the water migrated through porous clay under an external electric field (Probstein 1994; Li 2004). Manz et al. successfully separated two fluorescent dyes from background electrolytes using capillary electrophoresis (CE) in the early 1990s, and proved the possibility for the realization of a micro total analysis system (μTAS) (Manz et al. 1992). Based on the achievements of Manz's group, Jacobson et al. fabricated a glass microchip with a cross-column

geometry, and proposed an efficient separation technique through CE and external electric field (Jacobson et al. 1994). For a rapid analysis of multiple bio samples, Woolley et al. developed a capillary array electrophoresis, and performed high-speed DNA fragment separation and DNA genotyping on the chip (Woolley and Mathies 1994; Woolley et al. 1997). Using a non-aqueous CE system with a reversed electroosmotic flow, Jensen and Hansen separated lipophilic substances in the extracts of *Hypericum perforatum* L. (Jensen and Hansen 2002). Pedersen-Bjergaard and Rasmussen proposed an electro-membrane isolation (EMI) system for rapid sample pretreatment of biological fluids, and demonstrated that the system was good for isolation, enrichment, and clean-up of the required substances from complicated biological samples (Pedersen-Bjergaard and Rasmussen 2006). Through AC electroosmosis driven by non-contact external electrodes, Wang et al. showed an efficient mixing in a small microfluidic reservoir (<10 μl) (Wang et al. 2006).

Dielectrophoresis pioneered by Pohl in the 1970s (Pohl 1978; Jones 1995) has been widely studied for the development of microfluidic chips. Betts detected microorganisms harmful to the human body contained in a food using DEP and AC electrodes (Betts 1995). Hughes et al. investigated a correlation between an AC electric field frequency and DEP forces exerted on a particle, and reported a size and an array shape of electrodes for effectively controlling particle motions (Hughes et al. 1996). Jones examined the effects of electric field gradients generated by AC electrodes on particle dipole moment (Jones 1995). Based on the achievements, DEP combined with AC electrodes was applied to transport and control particles or cells. Using the electrodes of castellated, interdigitated, parallel, and polynomial geometries, Wang et al. described the dielectrophoretic behaviors of DS19 cells including trapping, levitation, and circulation (Wang et al. 1997). However, most works using DEP require complex fabrication procedures and configurations to integrate and maintain electrodes in a microfluidic chip, and to secure the flow path of a microchannel because of the limited area for the electrodes and the electrohydrolysis near them (Cummings and Singh 2003).

Cummings and Singh proposed a unique method to induce DEP without the integration of electrodes (Cummings and Singh 2003). They produced electric field gradients by arranging insulating posts in a microchannel and placing DC electrodes in reservoirs of a microfluidic chip, and then demonstrated DEP effects on 200 nm polystyrene particles with respect to three post shapes (circular, diamond, and square). In addition, Lapizco-Encinas et al. separated live and dead *E. coli*. cells using insulating posts and DEP effects (Lapizco-Encinas et al. 2004a).

A simultaneous application of EK and DEP probably make significant contributions to the development of on-chip sample pretreatment techniques. In general, the forces exerted on particles by EK and DEP are perpendicular, and combining the two phenomena may lead to convenient and effective particle controls in a microchannel. Particularly, DEP with a DC electric field and insulating posts allows an easy combination of EK and DEP in a microchannel due to the simple chip-design and fabrication procedure. However, a comprehensive study is required to realize a combination of EK and DEP for on-chip sample pretreatment.

This paper investigates the EK and DEP forces exerted on particles in a microchannel using numerical simulations, and proposes an improved geometry to enhance particle transports across EK streamlines. The microchannel has a circular post array which generates electric field gradient under an external DC electric field. To predict electric fields and particle flows, an in-house code is developed based on the results of Cummings and Singh (2003). The code is validated by comparing the results with those of Cummings and Singh. In addition, this paper describes the detailed theoretical background of EK and DEP, and discusses the criteria for characterizing particle flows with respect to the intensities of external electric fields.

2 Theoretical background

2.1 Electrokinesis and dielectrophoresis

Electrokinesis (EK), including electroosmosis and electrophoresis, is a particle and fluid transport phenomenon occurring when an external electric field is applied to an electrolyte in contact with solid surfaces, and its strength is proportional to the electric field intensity (Probstein 1994; Li 2004). Electroosmosis is the movement of a fluid driven by an external electric field relative to a stationary, charged, and solid surface. Generally, most substances acquire surface electric charges upon contact with an aqueous solution, and the charged surface influences the distribution of nearby ions in an electrolyte solution. While the co-ions of the surface charges are repelled from the surface, the counter ions are attracted toward the surface. This repulsion and attraction leads to the formation of a Debye layer above the surface. The mobile counter ions in the Debye layer move toward the counter-electrode upon the application of an external electric field. Due to the low Reynolds number of a microchannel flow, the migration of the counter ions causes the flow of the electrolyte fluid which is called electroosmosis.

An electroosmotic flow is assumed to have a one dimensional velocity profile to the first approximation, and its boundary condition is given by a slip condition. This is because the thickness of a Debye layer, typically of the order of $\sim$10 nm, is very small when compared to the characteristic length of a microchannel, and the velocity gradient is negligible in the Debye layer. The 1-D velocity profile is expressed by the Helmholtz–Smoluchowski relation as follows:

$$\vec{u}_{\mathrm{eo}} = \mu_{\mathrm{eo}}\vec{E}, \text{ and } \quad \mu_{\mathrm{eo}} = \frac{\varepsilon_{\mathrm{f}}\zeta_{\mathrm{w}}}{\eta_{\mathrm{f}}} \tag{1}$$

where $\vec{u}_{\mathrm{eo}}$ is the electroosmotic velocity, μ_{eo} is the electroosmotic mobility, and $\vec{E}$ is the local electric field intensity. ε_f, η_f, and ζ_{w} refer to the permittivity and the viscosity of a fluid, and the zeta potential of a microchannel wall, respectively.

Electrophoresis is defined as the movement of a charged particle relative to a stationary fluid driven by an external electric field. Depending on the Debye layer thickness (λ_{D}) relative to the particle's radius (r_{p}), the electrophoretic velocity is calculated as (Probstein 1994)

$$\vec{u}_{\mathrm{ep}} = \begin{cases} \mu_{\mathrm{ep}}\vec{E} & (\lambda_{\mathrm{D}} \ll r_{\mathrm{p}}) \\ \frac{2}{3}\mu_{\mathrm{ep}}\vec{E} & (\lambda_{\mathrm{D}} \gg r_{\mathrm{p}}) \end{cases} \tag{2}$$

$$\mu_{\mathrm{ep}} = \frac{\varepsilon_{\mathrm{f}}\zeta_{\mathrm{p}}}{\eta_{\mathrm{f}}} \tag{3}$$

where $\vec{u}_{\mathrm{ep}}$ and μ_{ep} are the electrophoretic velocity and mobility of a particle, respectively. ζ_{p} is the zeta potential of the particle surface.

Dielectrophoresis (DEP), occurring due to electric field gradient, is defined as the motion of either neutralized or charged particle with an induced dipole. When the electric field is uniform around a particle, the particle has no net electrostatic forces on it, resulting in no movement. When the electric field is non-uniform, however, a net electrostatic force is exerted on a particle in the direction of the gradient, and consequently causes the particle movement. The DEP velocity is expressed as follows (Pohl 1978; Probstein 1994; Jones 1995).

$$\vec{u}_{\mathrm{dep}} = \mu_{\mathrm{dep}}\nabla E^2 \quad \text{and} \quad \mu_{\mathrm{dep}} = \frac{r_{\mathrm{p}}^2}{3\eta_{\mathrm{f}}}\varepsilon_{\mathrm{f}}\mathrm{Re}[K(\omega)] \tag{4}$$

where $\vec{u}_{\mathrm{dep}}$ and μ_{dep} are the dielectrophoretic velocity and mobility of a particle. $Re\ [K(\omega)]$ is the real part of the Clausius-Mossotti factor (K) that is influenced by the frequency of an applied electric field.

The direction of a particle movement by DEP depends on the permittivity (or conductivity) difference between a particle and the surrounding fluid (Jones 1995). Based on the direction, DEP is categorized into positive DEP and negative DEP. When the permittivity (or conductivity) of a particle is larger than that of the surrounding fluid, the particle is attracted to the strong electric field, and it is called positive DEP. In contrast, the negative DEP, occurring when the fluid permittivity is larger, transports a particle toward the weak electric field.

2.2 Classification of particle flows driven by EK and DEP

Particle flows show a different behavior with respect to the intensity of an external DC electric field when EK, DEP, and particle diffusion occur together in a microchannel. The flows can be classified into three types (Cummings and Singh 2003): EK flow, streaming DEP flow, and trapping DEP flow. The EK flow is produced at a low electric field where particle transports are considerably affected by EK and diffusion because the effects of electric field gradient are weak. As a result, the particles move almost parallel to electric field lines. In a streaming DEP flows occurring at a moderate electric field, particles migrate along particular streamlines because the effects of DEP are balanced with the effects of EK and diffusion. Note that DEP is affected by the electric field squared, while EK is linearly proportional to the electric field according to Eqs. (1), (2) and (4). The DEP effects become stronger than the EK effects with an increase in the electric field. Finally, a trapping DEP flow occurs at a high electric field, and the flow is dominated by DEP. Most particles are trapped due to large DEP forces holding them against microchannel walls so that they cannot migrate downstream along with the fluid.

The three flow types can be distinguished by dimensionless variables that are derived by considering the directions of particle flux and electric field. For a dilute particle concentration, the effects of particle diffusion can be neglected, and the flux of particles driven by the external DC electric field is given as

$$\vec{j} = C(\vec{u}_{\mathrm{ek}} + \vec{u}_{\mathrm{dep}}) \tag{5}$$

where j is the particle flux, C is the particle concentration in a fluid, and $\vec{u}_{\mathrm{ek}}$ indicates the electrokinetic velocity of a particle. For an EK flow, $\vec{j}\cdot\nabla\vec{E} = 0$ since the particles migrate along with electric field lines. On the other hand, the particle motions are strongly governed by DEP in a trapping DEP flow, and the direction of particle flux is perpendicular to electric field lines, leading to $\vec{j}\cdot\vec{E} = 0$ (Lapizco-Encinas et al. 2004b). Therefore, the dimensionless variables for an EK flow and a trapping DEP flow can be expressed as follows:

For an EK flow,

$$\frac{\mu_{\text{dep}}\nabla(\vec{\text{E}}\cdot\vec{\text{E}})\cdot\nabla\vec{\text{E}}}{\mu_{\text{ek}}\vec{\text{E}}\cdot\nabla\vec{\text{E}}} \leq 1 \tag{6}$$

For a trapping DEP flow,

$$\frac{\mu_{\text{dep}}\nabla(\vec{\text{E}}\cdot\vec{\text{E}})\cdot\vec{\text{E}}}{\mu_{\text{ek}}\vec{\text{E}}\cdot\vec{\text{E}}} \geq 1 \tag{7}$$

A streaming DEP flow occurs at the electric field intensities where both Eqs. (6) and (7) are not satisfied.

3 Development of numerical program

3.1 Grid generation

For the numerical calculations of particle flows in a microchannel with a post array, grids are generated by elliptic PDE (Thomson et al. 1974) and the full boundary control method (Choi and Maeng 1999). The elliptic PDE is useful to obtain a desired distribution of grid points due to the high stability of the solution, and it allows effective controls on the orthogonality and the spacing of grid lines near boundaries. The full boundary control method makes it possible to automate the grid generation processes, and increases numerical stability because it keeps a control function value within a given range. Therefore, we were able to produce a good quality of grids by maintaining the diagonal dominance.

3.2 Governing equations and boundary conditions

To predict the particle and fluid flows in a microchannel driven by the external DC electric field, coupled Poisson and Navier–Stokes equations should be solved (Morrison 1970; Ermakov et al. 1998). However, this requires complex calculation processes and considerable computing loads. Instead, Cummings et al. (2000) proposed a simple mathematical model which decouples the calculations of the electric field and the velocity field. They used the Laplace equation in (8) for the calculations of the electric field and a simple relation in (9) for the calculations of the particle velocity field.

$$\nabla^2\phi = 0 \quad (\vec{E} = -\nabla\phi) \tag{8}$$

$$\vec{u}_{\text{p}} = \mu_{\text{eo}}\vec{E} - \mu_{\text{ep}}\vec{E} + \mu_{\text{dep}}\nabla(\vec{E}\cdot\vec{E}) \tag{9}$$

where ϕ is an electric potential field and $\vec{u}_{\text{p}}$ is the particle velocity by EK and DEP. This model is valid when the external electric field is steady (i.e., DC electric field), and the electric and physical properties of the fluid are constant. In addition, the Debye layer should be thin as compared to the characteristic length of a microchannel so that the Helmholtz–Smoluchowski relation in Eq. (1) is applicable to fluid–solid boundaries. Since most microchannel flows, including those in the present study, satisfy the above conditions under a DC electric field, we develop a numerical program based on this model. The inlet and outlet boundary conditions for the Laplace equation are such that the electric potential is uniform at the each boundary, and that the potential gradient is zero normal to the post surface, implying that the posts are electrically insulated.

3.3 Flow visualization by Monte-Carlo simulation

A Monte-Carlo simulation program is developed to visualize particle transports after calculating the particle velocities using Eq. (9). Assuming point particles and, consequently, no collisions between them, the particle flows are dominated by EK, DEP, and diffusion. While the EK and DEP effects on a particle velocity are considered in the calculations of particle velocities, the diffusion effects are determined during the Monte-Carlo simulations, considering the diffusion length and random directions. Also, a particle velocity is determined by the nearest neighbor scheme (Prevost et al. 2001; Atramentov and LaValle 2002), when its location happens to be in a grid mesh at a given time step. It assigns the velocity of the nearest grid point to the particle, considering the distance between a particle and the surrounding grid points.

4 Validation of the numerical program

In order to verify the results of the numerical program, we compared them with those of Cummings and Singh (2003). The reference flow geometry of the present study is identical to the microchannel they used, as shown in Fig. 1. It is assumed as a glass microchannel with circular posts with a 33 μm diameter arranged in squares. The posts induce electric field gradients upon the application of an external electric field. The particles injected to the microchannel are assumed to be carboxylated latex nanospheres of 200 nm in diameter, and the fluid is assumed as a 1 mM phosphate buffer of pH 7.7. The mobilities of μ_{eo}, μ_{ep}, and μ_{dep} in Eqs. (1), (3), and (4) are computed using the parameter values given in literatures (Morgan et al. 1999; Cummings and Singh 2003).

Figure 2 shows the electric potential distribution in the microchannel obtained from the Laplace equation when the electric field is 25 V/mm. Isopotential lines are curved due to the electrically insulated posts, and the electric field

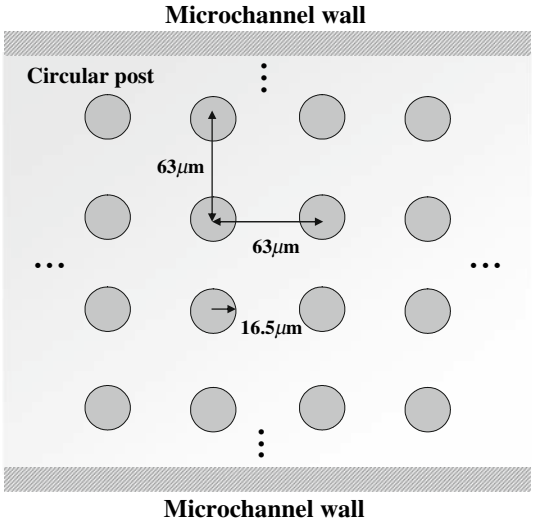

Fig. 1 The geometry of the reference microchannel

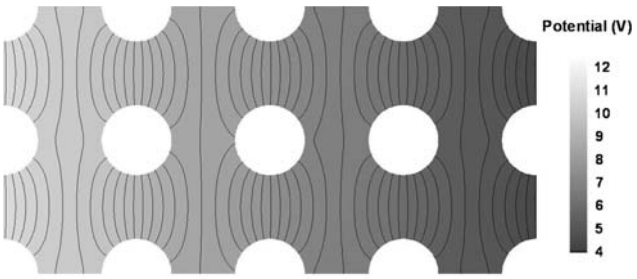

Fig. 2 The distribution of electric potential in the microchannel for an external electric field of 25 V/mm. The *curved lines* are isopotential lines

intensity is larger in a narrow path than in a wide path. This leads to a non-uniform electric field throughout the microchannel. The electric field would be uniform without the posts, resulting in a simple EK flow. However, the electric field gradients caused by the insulating posts generate DEP in the microchannel, making the flow governed by DEP as well as EK.

The particle velocity vectors induced by EK and DEP are plotted in Fig. 3a for an external electric field of 25 V/mm. Since this electric field is too weak to induce DEP in the microchannel, EK and diffusion dominate the particle flow so that it appears like a potential flow. For example, the particles in a narrow path have larger velocities than those in a wide path since the electric field intensity is greater. In contrast, DEP governs the particle flow when the electric field intensity becomes strong. Figure 3b shows the particle velocity vectors when the external electric field is 100 V/mm. The velocity vectors are directed toward the lateral sides of the circular posts where the electric field intensity is stronger than any other regions. This indicates that the particle flow shows a positive DEP because the conductance of particles (18.8 mS) is greater than that of fluids (18 mS).

Monte-Carlo simulations for the microchannel flows confirm the three types of particle flows (EK, streaming DEP, and trapping DEP) with respect to the intensity of electric field as reported by Cumming and Singh (2003). At a low electric field of 25 V/mm, particles are almost evenly spread in the microchannel moving downstream, as shown in Fig. 4a. Also, the distribution of pathlines is regularly repeated through the microchannel, and is symmetric about the centerline of the microchannel. This is because the flow is considerably governed by EK and diffusion. When the electric field increases to 80 V/mm, a streaming DEP flow occurs as shown in Fig. 4b. Particles move along particular streamlines aligned with the surface of posts. This is because DEP is balanced with EK and diffusion. While particles are transported downstream by EK, they are simultaneously attracted toward the post surfaces by DEP forces, which can be identified in the pathline plot. Figure 4c shows a trapping DEP flow occurring at a high electric field of 100 V/mm. Particles do not migrate

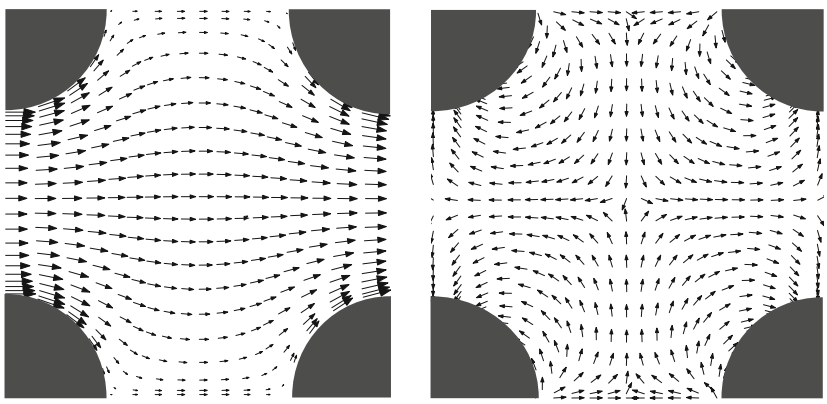

Fig. 3 The velocity vectors of particles in a microchannel. The particle velocities are obtained from Eq. (9)

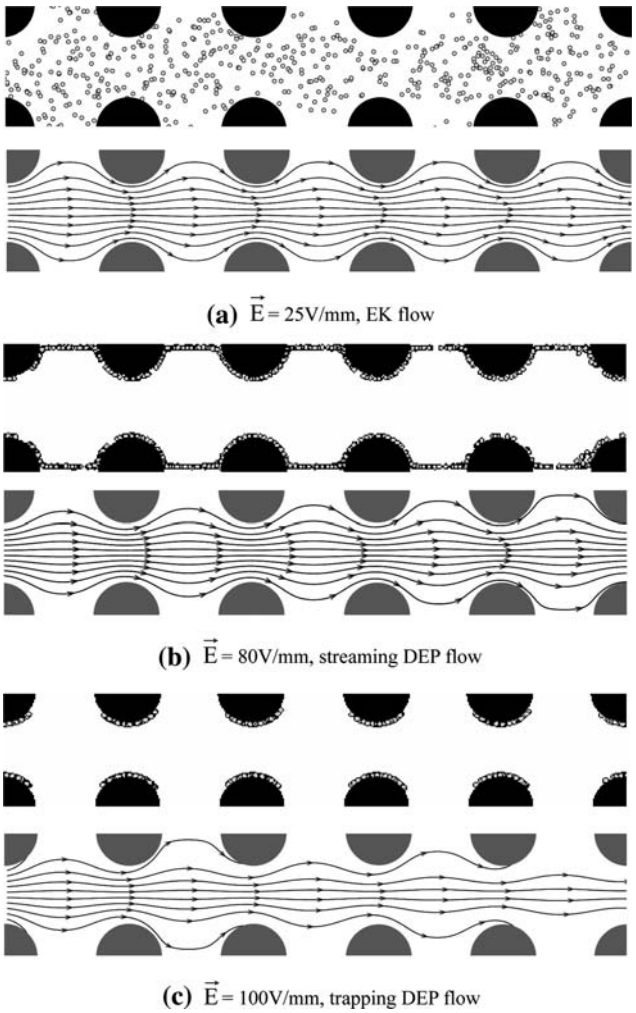

Fig. 4 The three particle flow types driven by the external DC electric field. *Top figures* in **a–c** are obtained from Monte-Carlo simulations and the *bottoms* show the pathlines of particles

downstream with the fluid, and are trapped locally on the circular post surface by strong DEP forces. While a particle moves downstream near the center region of the microchannel, it is gradually attracted toward the post surfaces. Then the particle is trapped upon entering the region of a strong electric field gradient, as clearly shown in the pathline plot. The results of Monte-Carlo simulations are in good agreement with the findings of Cummings and Singh, and imply that the numerical program developed in the present study can accurately predict a microchannel flow driven by EK, DEP, and diffusion.

5 Improvement of microchannel geometry for particle separation

We investigate the EK and DEP forces exerted on particles in a microchannel with a circular post array, and improve the channel geometry for rapid particle separation by maximizing lateral forces on particles. The reference geometry is the microchannel used for the validation of the numerical program.

5.1 Variations of EK and DEP forces with microchannel geometries

In order to examine the effects of the microchannel geometry on particle transports in a microchannel with a circular post array, the EK and DEP forces in a unit cell of the flow geometry are divided into longitudinal and lateral components as shown in Fig. 5. The average force ratio (FR) of the lateral to longitudinal components per unit cell is defined as follows:

$$\mathrm{FR}(R, L_1, L_2) = \frac{1}{A}\int \left|\frac{F_{\mathrm{ek}.y} + F_{\mathrm{dep}.y}}{F_{\mathrm{ek}.x} + F_{\mathrm{dep}.x}}\right| \mathrm{d}A \tag{10}$$

where R is the radius of a post, and L_1 and L_2 denote the longitudinal and lateral spacings between neighboring posts. The unit cell area is denoted by A. $\vec{F}_{\mathrm{ek}}$ and $\vec{F}_{\mathrm{dep}}$ defined in Eqs. (11) and (12) represent the electrokinetic and dielectrophoretic forces in Cartesian coordinates, respectively.

$$\vec{F}_{\mathrm{ek}} = 6\pi r_{\mathrm{p}} \varepsilon_{\mathrm{f}} (\zeta_{\mathrm{w}} - \zeta_{\mathrm{p}}) \vec{E} \tag{11}$$

$$\vec{F}_{\mathrm{dep}} = 2\pi r_{\mathrm{p}}^3 \varepsilon_{\mathrm{f}} \mathrm{Re}[K(\omega)] \nabla E^2 \tag{12}$$

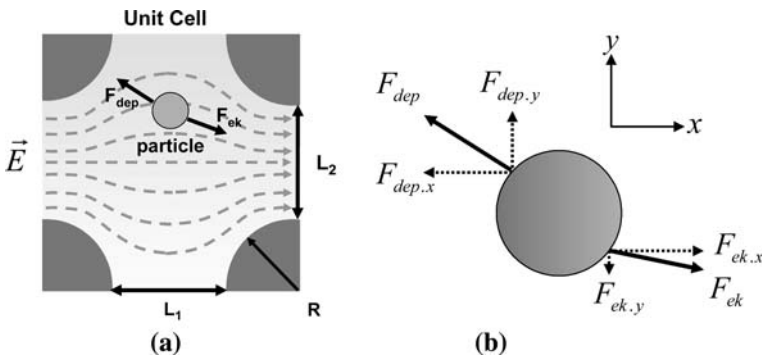

Fig. 5 Geometric parameters of a microchannel with circular posts (**a**) and forces exerted on a particle by EK and DEP (**b**)

FR can be used to maximize the rate of particle transport toward the posts for a given power dissipation per unit cell. A larger value of FR implies that a particle near the centerline of a microchannel would deviate quicker toward the post. Thus, a microchannel geometry with a large value of FR would be more suitable for on-chip sample pretreatment to separate particles from the fluid.

Figure 6 shows the variation of FR with respect to the ratio of the longitudinal post spacing to the post radius for various values of the lateral post spacing normalized by the longitudinal length of a unit cell. The value of FR is maximized when L_1/R is about 0.6 for all values of $L_2/(L_1 + 2R)$. The maximum FR occurring at $L_1/R = 0.6$ is probably because the region of the unit cell is too small to form a strong electric field gradient when the circular posts are too close to one another. We did not consider the microchannel geometry with a lower value of $L_2/(L_1 + 2R)$ than 0.1 since a too large aspect ratio would result in excessive Joule heating caused by a high electric field intensity.

5.2 Improvement in microchannel geometry

We improve the reference microchannel based on the prementioned results so that the longitudinal post-spacing is 0.6 times the post radius, keeping the other geometric parametric ratios the same as the reference. Figure 7 compares the reference and improved microchannels. To investigate the performance of the two microchannels, we conducted Monte-Carlo simulations to count the number of particles passing through the three unit cells of two microchannels.

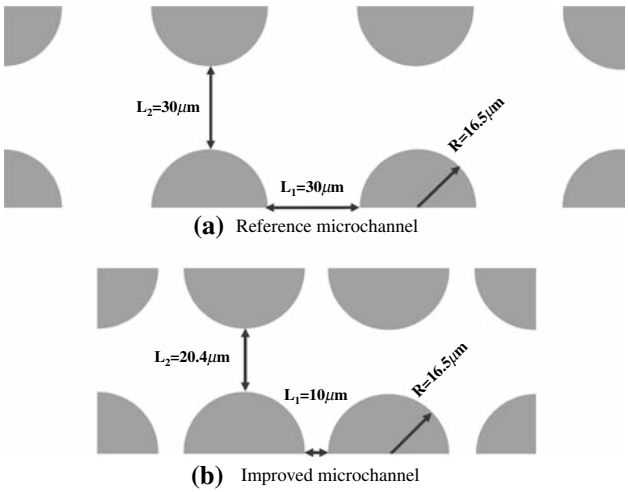

Fig. 7 Comparison of the reference and improved microchannels. They are drawn to scale for convenient comparison. The values of $L_2/(L_1 + 2R)$ remains the same between the two microchannels

Figure 8 shows the percentage ratio of the number of particles passing through the outlet of the three unit cells as compared to the number at the inlet for the variation of external electric field intensities. The particles were distributed evenly at the inlet, and the three unit cells were selected to observe accumulated DEP effects. The ratio starts to significantly decrease beyond 60 V/mm for the improved microchannel, while it shows a significant reduction beyond 80 V/mm for the reference microchannel. This means that the improved microchannel traps particles better than the reference channel due to a stronger lateral force for the same intensity of external electric field.

To investigate the details of particle migration toward the post surfaces due to lateral forces, we divided the microchannel into the post region (A) and the center region (B), as shown in Fig. 9a. The width ratio of the post to

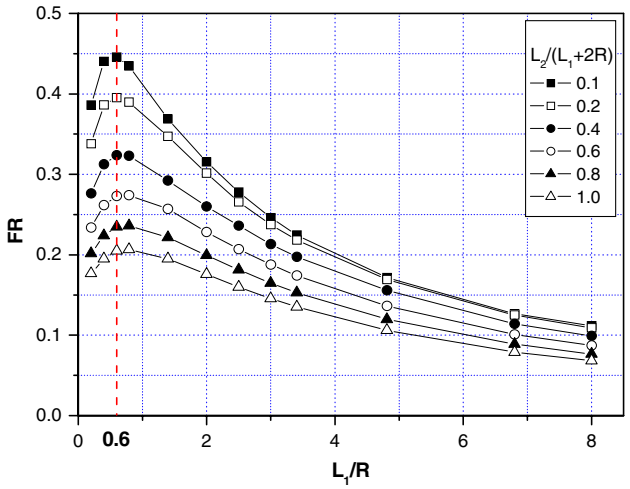

Fig. 6 The variation of force ratio (FR) with respect to geometric parameters. The post radius is 16.5 μm

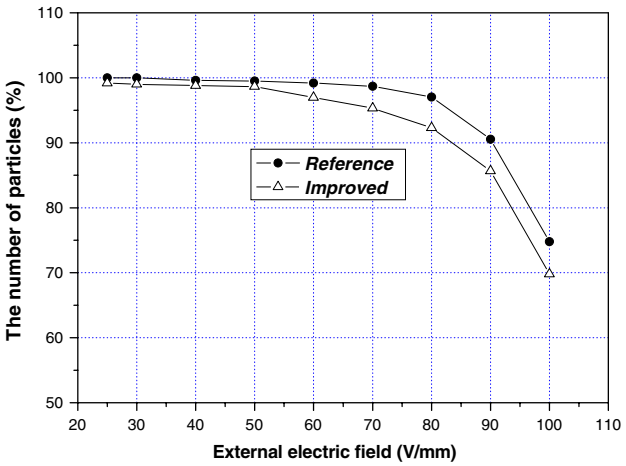

Fig. 8 The percentage ratio of the number of particles at the outlet to that at the inlet

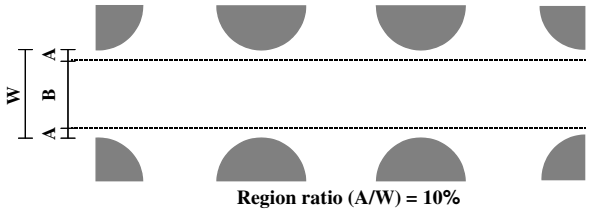

(a) The center and post regions in a microchannel.

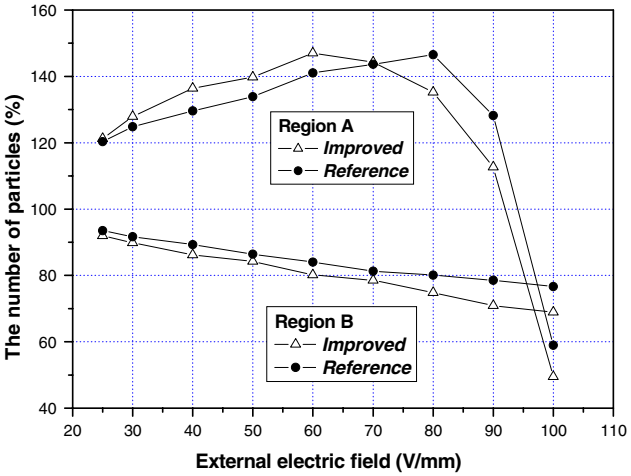

(b) The percentage rate variations of the number of particles for the center and post regions.

Fig. 9 Comparison of particle flows between the improved and reference microchannels

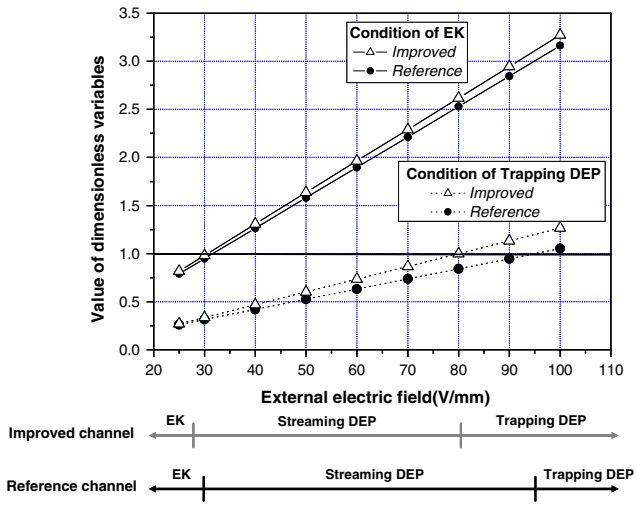

Fig. 10 The variation of dimensionless variables for improved and reference microchannels with respect to the external electric field

center regions is 10% at the narrowest path. Figure 9b shows the percentage ratio of the number of particles for the two regions of each microchannel. The results suggest that the improved microchannel has a significantly small number of particles in the center region of the outlet beyond 70 V/mm because of the stronger lateral forces, as compared to the reference microchannel. In the post region of the improved microchannel, the percentage ratio rapidly increases until 60 V/mm, indicating that the number of particles entering the post region is larger than that trapped on the post. This implies that the electric field intensity around 60 V/mm results in a streaming DEP flow. Beyond this value, the percentage rate decreases, and the number of particles in the post region of the outlet becomes smaller at 100 V/mm than that of the inlet, resulting in a trapping DEP flow. On the other hand, the reference microchannel exhibits a similar trend, but the percentage ratio increases until 80 V/mm because the DEP effects are weak as compared to the improved microchannel.

The dimensionless variables defined in Eqs. (6) and (7) are applied to the two microchannels to examine electric field intensities that distinguish an EK flow and a trapping DEP flow. The variables are averaged over a unit cell area of the two microchannels for comparison as follows:

For EK flows,

$$\frac{1}{A}\int\left|\frac{\mu_{\mathrm{dep}}\nabla(\vec{E}\cdot\vec{E})\cdot\nabla\vec{E}}{\mu_{\mathrm{ek}}\vec{E}\cdot\nabla\vec{E}}\right|\mathrm{d}A \tag{13}$$

For trapping DEP flows,

$$\frac{1}{A}\int\left|\frac{\mu_{\mathrm{dep}}\nabla(\vec{E}\cdot\vec{E})\cdot\vec{E}}{\mu_{\mathrm{ek}}\vec{E}\cdot\vec{E}}\right|\mathrm{d}A \tag{14}$$

Figure 10 shows the values of two dimensionless variables with respect to the external electric field intensities. Both values increase linearly with the electric field, and there exists ranges of the electric field that satisfy the condition of an EK flow or a trapping DEP flow. The results suggest that EK dominates the particle flows when the electric field intensity is below 30 V/mm for both microchannels. However, a critical value for trapping DEP is different for the two microchannels: 80 V/mm for the improved microchannel and 95 V/mm for the reference microchannel. It should not be interpreted that a trapping DEP flow occurs only when the value of Eq. (14) is greater than 1 since the values of the dimensionless variables were averaged over a unit cell area. The results indicate that the improved microchannel strengthens the DEP effects at an intensity of the external electric field as compared to the reference microchannel. In other words, the improved microchannel requires a lower electric field intensity to achieve the same DEP effects than the reference microchannel does, and enhances particle transports across EK streamline for a given power dissipation per unit cell. Therefore, the improved microchannel would result in better particle separations and less Joule heating than the reference microchannel, which is critical in an application of a microfluidic chip for biochemical analysis.

6 Conclusions

We developed an in-house numerical program to predict EK and DEP in a microchannel, and presented an improved microchannel geometry for enhanced particle transports across EK streamline for a given power dissipation. The numerical program consists of grid generation using the elliptic PDE and the full boundary control method, Laplace equation solver, and Monte-Carlo simulation for flow visualization. The program was validated against the findings of Cummings and Singh (2003), and the three particle flow types that they suggested were identified. To improve a microchannel geometry with a circular post array, we defined a force ratio of lateral to longitudinal components exerted on a particle by EK and DEP. The results indicated that the force ratio has the maximum value when the longitudinal spacing between the posts is 0.6 times the post radius. The improved microchannel exhibited stronger DEP effects than the reference microchannel, implying that it can separate particles more effectively. The dimensionless variables that distinguish particle flow types also confirmed that the improved microchannel requires a less external electric field than the reference microchannel does to achieve the same DEP effects.

The numerical program can be used to design or optimize a microchannel geometry for on-chip sample pretreatment like particle separation using EK and DEP. Generally, DEP requires a high electric field intensity resulting in the excessive Joule heating and denaturation of bio molecules like proteins. However, this paper indicated that a low electric field might be used to obtain the desired DEP effects through a smart design of a microchannel with numerical simulations.

Acknowledgments This work was financially supported by the Future-Oriented Core Research Fund (2E19570) from the Korea Institute of Science and Technology (KIST) and the Korea Research Foundation Grant (KRF-2006-331-D00069) funded by the Korean Government (MOEHRD).

References

Atramentov A, LaValle SM (2002) Efficient nearest neighbor searching for motion planning. IEEE Trans Rob Autom 1:632–637

Auroux P-A, Iossifidis D, Reyes DR, Manz A (2002) Micro total analysis systems. 2. Analytical standard operations and applications. Anal Chem 74:2637–2652

Betts WB (1995) The potential of dielectrophoresis for the real-time detection of microorganisms in foods. Trends Food Sci Tech 6:51–58

Choi IK, Maeng JS (1999) Automated body-fitted grid generation method with application to natural convection problem. Trans KSME(B) 23(6):703–712

Cummings EB, Singh AK (2003) Dielectrophoresis in microchips containing arrays of insulating posts : theoretical and experimental results. Anal Chem 75:4724–4731

Cummings EB, Griffiths SK, Nilson RH, Paul PH (2000) Condition for similitude between the fluid velocity and electric field in electroosmotic flow. Anal Chem 72:2526–2532

Ermakov SV, Jacobson SC, Ramsey JM (1998) Computer simulations of electrokinetic transport in microfabricated channel structures. Anal Chem 70(21):4494–4504

Hughes MP, Pethig R, Wang X-B (1996) Dielectrophoretic forces on particles in travelling electric fields. J Phys D Appl Phys 29:474–482

Jacobson SC, Hergenroder R, Koutny LB, Ramsey M (1994) High-speed separations on a microchip. Anal Chem 66:1114–1118

Jensen AG, Hansen SH (2002) Separation of hypericins and hyperforins in extracts of hypericum perforatum L. using non-aqueous capillary electrophoresis with reversed electro-osmotic flow. J Pharm Biomed Anal 27:167–176

Jones TB (1995) Electromechanics of particles. Cambridge University Press, London

Lapizco-Encinas BH, Simmons BA, Cummings EB, Fintschenko Y (2004a) Dielectrophoretic concentration and separation of live and dead bacteria in an array of insulators. Anal Chem 76:1571–1579

Lapizco-Encinas BH, Simmons BA, Cummings EB, Fintschenko Y (2004b) Insulator-based dielectrophoresis for the selective concentration and separation of live bacteria in water. Electrophoresis 25:1695–1704

Li D (2004) Electrokinetics in microfluidics. Elservier Academic Press, London

Manz A, Harrison DJ, Verpoorte EMJ, Fettinger JC, Paulus A, Ludi H, Widmer HM (1992) Planar chips technology for miniaturization and integration of separation techniques into monitoring systems: capillary electrophoresis on a chip. J Chromatogr 593:253–258

Morgan H, Hughes MP, Green NG (1999) Separation of submicron bioparticles by dielectrophoresis. Biophys J 77:516–525

Morrison FA (1970) Electrophoresis of a particle of arbitrary shape. J Colloid Interface Sci 34(2):210–214

Pedersen-Bjergaard S, Rasmussen KE (2006) Electrokinetic migration across artificial liquid membranes : new concept for rapid sample preparation of biological fluids. J Chromatogr A 1109:183–190

Pohl HA (1978) Dielectrophoresis: the behavior of neutral matter in nonuniform electric fields. Cambridge University Press, London

Prevost M, Edwards MG, Blunt MJ (2001) Streamline tracing on curvilinear structured and unstructured grids. Proc Society Petroleum Eng

Probstein RF (1994) Physicochemical hydrodynamics: an introduction. Wiley, New York

Reyes DR, Iossifidis D, Auroux P-A, Manz A (2002) Micro total analysis systems. 1. Introduction, theory, and technology. Anal Chem 74:2623–2636

Thomson JF, Thames FC, Mastin CW (1974) Automatic numerical generation of body-fitted curvilinear coordinate system for field containing any number of arbitrary two-dimensional bodies. J Comput Phys 59:151–163

Vilkner T, Janasek D, Manz A (2004) Micro total analysis system. Recent developments. Anal Chem 76:3373–3386

Wang X-B, Huang Y, Gascoyne PRC, Becker FF (1997) Dielectrophoretic manipulation of paticles. IEEE Trans Ind Appl 33(3):660–669

Wang S-C, Chen H-P, Lee C-Y, Yu C-C, Chang H-C (2006) AC electro-osmotic mixing induced by non-contact external electrodes. Biosens Bioelectron 22:563–567

Woolley AT, Mathies RA (1994) Ultra-high-speed DNA fragment separations using microfabricated capillary array electrophoresis chips. Proc Natl Acad Sci USA 91:11348–11352

Woolley AT, Sensabaugh GF, Mathies RA (1997) High-speed DNA genotyping using microfabricated capillary array electrophoresis chips. Anal Chem 69:2181–2186